

ARTICLE

Suppression of surface waves in seismic data using an adaptive time–frequency–wavenumber filter

Xuejie Gao^{1,2} , Yong Wang^{1,2*}, Youjuan He³, Zhili Chen^{1,2}, Zerun Nian⁴, and Lang Yang⁴¹Department of Geophysical Exploration, School of Geophysics and Petroleum Resources, Yangtze University, Wuhan, Hubei, China²Key Laboratory of Oil and Gas Resources and Exploration Technology, Yangtze University, Wuhan, Hubei, China³Research Institute of Exploration and Development, Northwest Oilfield Company, SINOPEC, Urumqi, Xinjiang Uygur Autonomous Region, China⁴Exploration and Development Research Institute, Geophysical Research Department, PetroChina Tarim Oilfield Branch, Korla, Xinjiang Uygur Autonomous Region, China

Abstract

Surface waves are a prevalent form of coherent interference in seismic recordings, characterized by low frequency, high energy, and slow velocity, which can significantly affect seismic data processing. Currently, surface wave suppression is primarily achieved by leveraging the differences between surface waves and signal waves in the frequency, amplitude, and wavenumber domains. Among these methods, frequency–wavenumber (FK) filtering is widely used. However, it requires manual selection of regions during filtering, which becomes challenging when processing large volumes of seismic data. Therefore, adaptive surface-wave suppression methods are essential for practical data processing. FK filtering transforms data into the FK domain to suppress linear noise. However, because surface waves are dispersive and exhibit partial nonlinearity, FK filtering alone is insufficient to fully suppress them. To address these issues, this study introduces a temporal dimension into the FK domain, leading to the development of the time–frequency–wavenumber (TFK) transformation. This transformation further separates surface and signal waves in the time domain, thereby mitigating dispersion. Moreover, it facilitates adaptive filtering of seismic data across different time intervals in the FK domain. By cross-correlating FK data from different time periods, adaptive filters were derived for each interval, which were then applied to obtain filtered seismic records. Comparisons between synthetic and real-world data demonstrated that our approach effectively suppresses surface waves while preserving the relative amplitude characteristics of signal waves.

Keywords: Seismic noise suppression; Surface-wave suppression; Frequency dispersion; Frequency–wavenumber filter; Adaptive time–frequency–wavenumber filtering; Cross-correlation

***Corresponding author:**Yong Wang
(cdwangyong@yangtzeu.edu.cn)

Citation: Gao X, Wang Y, He Y, Chen Z, Nian Z, Yang L. Suppression of surface waves in seismic data using an adaptive time–frequency–wavenumber filter. *J Seismic Explor.* 2026;35(2):025450103. doi: 10.36922/JSE025450103

Received: November 5, 2025**Revised:** February 9, 2026**Accepted:** February 12, 2026**Published online:** April 27, 2026

Copyright: © 2026 Author(s). This is an Open-Access article distributed under the terms of the Creative Commons Attribution License, permitting distribution, and reproduction in any medium, provided the original work is properly cited.

Publisher's Note: AccScience Publishing remains neutral with regard to jurisdictional claims in published maps and institutional affiliations.

1. Introduction

Noise suppression holds significant importance in petroleum seismic exploration, as it exerts a notable influence on subsequent processing. Seismic data are predominantly affected by diverse wave types, with surface waves being prominent. Surface waves feature a fan-shaped distribution, characterized by high energy, low frequency, slow velocity, and frequency dispersion.^{1,2} Their presence conceals seismic reflections that are vital for mapping subsurface structures. This concealment effect not only complicates the extraction of valuable geological information but also heightens the risk of misinterpretation, thereby directly affecting the accuracy of hydrocarbon reservoir evaluations and geological hazard assessments. Conventional methods aimed at alleviating this effect often encounter challenges. They struggle to effectively separate and suppress surface waves while safeguarding the integrity of seismic signals.³

Surface waves can be grouped into Rayleigh and Love waves. A Rayleigh wave is a seismic surface wave produced by the interference between surface longitudinal and transverse waves. On the other hand, Love waves originate when S-waves travel along layered interfaces. Both kinds of waves propagate along the surface.⁴ In the realm of petroleum seismic exploration^{5,6}, these waves are usually suppressed. However, in engineering seismic exploration, they are used for tasks such as determining crack morphology and detecting in-situ damage.⁷⁻⁹ In petroleum seismic exploration, vertical-component geophones are commonly used, which results in the reception of Rayleigh waves. Therefore, this research centers on Rayleigh surface waves.

Traditional approaches for attenuating surface waves primarily include high-pass filters, frequency-wavenumber (FK) filters, and time-intercept slowness filters. Although these approaches are somewhat efficient and effective, each has distinct drawbacks.¹⁰ As a result, in recent years, a variety of surface wave analysis methods have emerged, such as the K-L transform, the slant FK filter, and deep learning techniques.¹¹⁻¹³ For example, Jin *et al.*¹⁴ put forward a new inverse dispersion method. This method addresses the nonlinearity caused by surface wave dispersion, enabling subsequent surface wave suppression through FK filtering. Liu *et al.*¹⁵ proposed a method integrating a blind-trace scheme and a self-supervised neural network. Its purpose is to eliminate aliased cone-shaped surface waves in seismic data. Lv *et al.*³ introduced a nonsubsampling Shearlet transform method. First, it conducts a preliminary separation of surface waves and effective waves. Then, the shearlet transform is used to decompose the data into multiple sub-bands. After that, correlation calculations

are performed to adaptively select the effective sub-bands. Lastly, an inverse transform is applied to the selected sub-bands. In response to the instability of the U-Net and related issues, Son *et al.*¹⁶ proposed the blind horizon network and dual-model self-supervised selective learning. Yuanyuan *et al.*¹⁰ presented a novel model-based, data-driven method for the attenuation of surface waves. This approach uses surface wave dispersion curve analysis and a joint inversion that combines the genetic algorithm and the conjugate gradient algorithm to develop a precise surface wave model. Subsequently, the model data are subtracted from the seismic data to enhance the signal-to-noise ratio.

Recent research indicates that the focus has mainly been on adaptivity and data analysis. Drawing on traditional methods, this study explores adaptive strategies to further advance the field's development. Yablokov *et al.*¹⁷ developed a novel approach for determining static corrections for the hodograph rectification of surface waves in the time-frequency (TF) domain. This method also involves preprocessing, in which the reflected wave signals are removed in advance.

The FK filtering technique differentiates between surface waves and reflected waves by exploiting their frequency and apparent velocity differences. In specific situations, it can efficiently reduce linear noise.^{18,19} Nevertheless, when surface and reflected waves show aliasing in the FK domain, or when the strong dispersion of surface waves diminishes their linear features, the performance of FK filtering is notably reduced. Numerous researchers have introduced the time-frequency-wavenumber (TFK) method by enhancing certain attributes to improve upon the original FK filtering approach. For instance, Askari and Siahkoobi²⁰ proposed the TFK method, which incorporates time information into the FK framework. By establishing different suppression areas in the FK domain at various time intervals, this method boosts surface wave suppression. Liu and Fomel²¹ proposed the I-TFK method. This method first applies the TFK transformation to the seismic data and then decomposes it using regularization techniques. Nonetheless, TFK filtering requires manual definition of a rejection zone at each time point. This poses a challenge when dealing with a large amount of seismic data. To address this issue, Wang and Wang²² proposed a polarization filtering approach based on the TFK method. This method creates an analytic signal by combining the horizontal and vertical amplitudes and automatically determines the rejection zone using the inverse of the ellipticity, thereby suppressing surface waves. However, this method is not suitable for data that comprise only vertical components. Wu *et al.*²³ proposed an automatic

data selection method for surface wave imaging, which is based on the energy distribution characteristics in the FK domain. Sun *et al.*²⁴ employed FK filtering to suppress single-frequency noise and linear noise and evaluated its excellent amplitude-preserving ability.

This paper presents an adaptive TFK filter to address the challenges of automatic filter configuration and the overlap between surface and effective waves, thereby improving surface wave suppression. In traditional FK filtering, accurately picking the surface wave region is a crucial step. However, conventional picking methods often fall short when dealing with the overlapping areas of surface and effective waves. These methods are unable to precisely delineate the boundaries of surface waves in such complex regions, resulting in incomplete suppression and potential distortion of the effective wave components. To address this limitation, an adaptive TFK filter was proposed. Initially, the TFK method was applied to seismic data containing surface waves, thereby acquiring data in the TFK domain. After that, cross-correlation operations were performed on the data in the FK domain across different time dimensions to obtain an adaptive filter. This adaptive filter could intelligently identify and separate surface wave components, even in overlapping areas, providing a more accurate filtering effect than traditional methods. Finally, the filters were applied to the FK domain data at various time points. Subsequently, an inverse TFK transformation was performed, resulting in the data with surface waves suppressed. Our approach can be used for both synthetic data and actual seismic records. By comparing it with the traditional FK filtering method, the remarkable advantages of the adaptive TFK filter were demonstrated.

2. Materials and methods

2.1. Time–frequency–wavenumber transformation

The TFK transformation is a signal-processing approach for extracting TFK information from seismic data. This methodology extends the FK transformation by integrating time information. Motivated by the S-transform-based ground-roll suppression approach validated by Askari and Siahkoobi²⁰, we applied the S-transform to each seismic trace within a shot gather to obtain a frequency-adaptive, multi-resolution TF representation. This frequency-dependent resolution is particularly suitable for land seismic data, where surface waves are typically non-stationary and exhibit strong dispersion—often characterized by low frequencies and long durations. In contrast, reflection events tend to manifest as more transient, higher-frequency features. Consequently, fixed-window TF representations, such as the short-time Fourier transform, may suffer from inherent trade-offs

between temporal and spectral resolution. Furthermore, the S-transform preserves a physically meaningful Fourier frequency axis and retains the full complex spectrum, enabling seamless integration with subsequent spatial Fourier transforms. This compatibility naturally supports the correlation-based operations performed on constant-frequency (FK) slices in our TFK-domain workflow.

The S-transform²⁵ is a method that represents a signal as a 2D function of frequency and time, enabling simultaneous observation of its characteristics in both domains. It employs a window function in the frequency and time domains to locally weight the signal and transform it at different times and frequencies. This results in a TF representation that shows the signal's energy distribution across time and frequency. The equation is as follows:

$$S(\tau, f) = \frac{|f|}{\sqrt{2\pi}} \int_{-\infty}^{+\infty} r(t) e^{\left[-\frac{1}{2}(\tau-t)^2 f^2\right]} e^{-i2\pi ft} dt \quad (1)$$

where $r(t)$ is the seismic data of a single trace, t and τ represent the time variables for the single-trace seismic data and the TF spectral data, respectively, f represents the frequency, i represents the imaginary part of the signal, and $S(\tau, f)$ represents the TF spectral data of the seismic signal.

After performing the S-transform on each trace of the seismic data, $S(\tau, f, c)$ is obtained, where c is the spatial variable of the seismic data, representing the offset distance. A Fourier transform is performed in the spatial direction to convert spatial information into wavenumber information. The equation is as follows:

$$\bar{S}(\tau, f, k) = \frac{1}{2\pi} \int S(\tau, f, c) e^{-i2\pi kc} dc \quad (2)$$

where $\bar{S}(\tau, f, k)$ represents the TFK transformation, which includes the results of time, frequency, and wavenumber, and k denotes the spatial wavenumber.

Since spatial sampling is often irregular in practical seismic data acquisition, appropriate adjustments to **Equation 2** are required when performing the spatial Fourier transform. In seismic data processing, irregular sampling can lead to spectral leakage and aliasing artifacts in the FK domain.²⁶ To mitigate these effects, we adopted an antileakage Fourier transform-based weighting scheme by introducing an integral weight $w(c_j)$ on irregular samples $\{c_j\}_{j=1}^N$, and discretized **Equation 2** as:

$$\bar{S}(\tau, f, k) = \frac{1}{\Delta X} \sum_{j=1}^N \left[w(c_j) \bar{S}(\tau, f, c_j) e^{-2\pi i k c_j} \right], \quad (3)$$

$$\bar{S}(\tau, f, c_j) = \bar{S}(\tau, f, k) e^{2\pi i k c_j}$$

where $w(c_j)$ is the integral weight, which is the reciprocal

of the sampling density; ΔX is a normalization factor involving the summation of all the sampled integral weights; and N is the number of input points.

2.2. Adaptive time–frequency–wavenumber filter

The adaptive TFK filtering technique suppresses surface waves in the TFK domain. After dispersion inversion processing, surface waves exhibit linear characteristics, and their energy is typically significantly stronger than that of effective waves. According to the convolution theorem, cross-correlation in the time domain corresponds to conjugate multiplication in the frequency domain. To accurately identify the distribution range of surface waves in the FK domain, this study computed FK characteristics corresponding to different time points to construct a discriminative weighting function. Specifically, by performing multiplicative operations on signals from adjacent time points in the TF domain, the cross-correlation in the time–space domain was calculated, thereby generating the weighting coefficients required for subsequent adaptive filtering. The specific equation is as follows:

$$w(\tau, f, k) = \sum_{i=\tau-\delta}^{\tau+\delta} |\bar{S}(\tau, f, k) \cdot \text{conj}(\bar{S}(i, f, k))| \quad (4)$$

where $w(\tau, f, k)$ is a correlation-based attribute used to characterize the relative strength and likelihood of surface wave energy at the TFK-domain coordinate (τ, f, k) ; τ denotes a discrete time-sample index along the time dimension of the TFK transform, serving as the center of a local correlation window; and δ denotes the half-window length in samples (an integer index offset after rounding), which controls the number of neighboring time samples involved in **Equation 4**. Accordingly, the full window length corresponds to $(2\delta+1)$ samples, i.e., $(2\delta+1)\Delta t$ in time with $\Delta t = 1/f_s$. In this study, the window length was designed to cover approximately four cycles of the dominant surface wave frequency f_0 , leading to **Equation 5**.

$$\delta = \text{round}\left(\frac{2f_s}{f_0}\right) \quad (5)$$

where f_s is the sampling frequency, f_0 is the dominant frequency of the surface wave, and $\text{round}(\cdot)$ denotes rounding to the nearest integer to ensure δ is an integer sample offset.

After performing the correlation calculations, $w(\tau, f, k)$ still contains regions of effective waves, necessitating additional refinement of $w(\tau, f, k)$. Since the inverse-dispersed surface waves exhibit linear characteristics and have the highest energy, a linear scan of $w(\tau, f, k)$ was conducted to identify the region with peak energy as the

surface wave area, while other regions were classified as non-surface wave areas. The equation is as follows:

$$w_0(k, f) = \begin{cases} 1 & |af - k| < \frac{4\pi f_0}{v} \\ 0 & \text{other} \end{cases} \quad (6)$$

where w_0 is the computational region, a is the surface wave slope obtained from energy scanning, and v is the velocity of surface waves. It should be noted that the surface wave slope a here is not a globally physically precise surface wave propagation velocity, but a locally valid approximation within short-time windows in the TFK domain. It is used only to initially constrain the candidate surface wave region, and local slope fluctuations have a limited impact on the final separation result.

A computational region is obtained through linear scanning and is then multiplied by the stacking area for further refinement. The refined stacking area is subsequently subjected to inverse computation to derive the final filtering region. Finally, filtering is performed in the TFK domain.

$$s_0(t, c) = \text{itfk} \left(\sum_{j=1}^T (\bar{S}(j, f, k) \cdot (1 - w)) \right) \quad (7)$$

where itfk is the inverse TFK, and $s_0(t, c)$ represents the data after surface wave suppression.

To clarify the overall processing procedure, the main steps of the proposed adaptive TFK filter are summarized in **Figure 1**.

As shown in **Figure 1**, the input shot gather in the time-offset domain is first transformed into the TFK spectrum by combining the S-transform in the TF domain with the spatial Fourier transform along the offset direction. Then, for each frequency and wavenumber, a time-windowed cross-correlation is computed between adjacent time slices of the TFK spectrum. This operation enhances the coherent and energetic components, primarily surface waves, and yields a correlation attribute that characterizes the strength of surface wave energy in the TFK domain. The correlation attribute is subsequently normalized to construct an adaptive TFK filter, which delineates the surface wave cone while preserving the reflection-dominated region. Finally, the adaptive filter is applied to the TFK spectrum, and the denoised shot gather is obtained in the time-offset domain by performing the inverse spatial Fourier transform together with the inverse S-transform.

3. Results

In this study, both synthetic and field seismic datasets were used to systematically compare the conventional FK filtering technique with the proposed adaptive TFK filtering

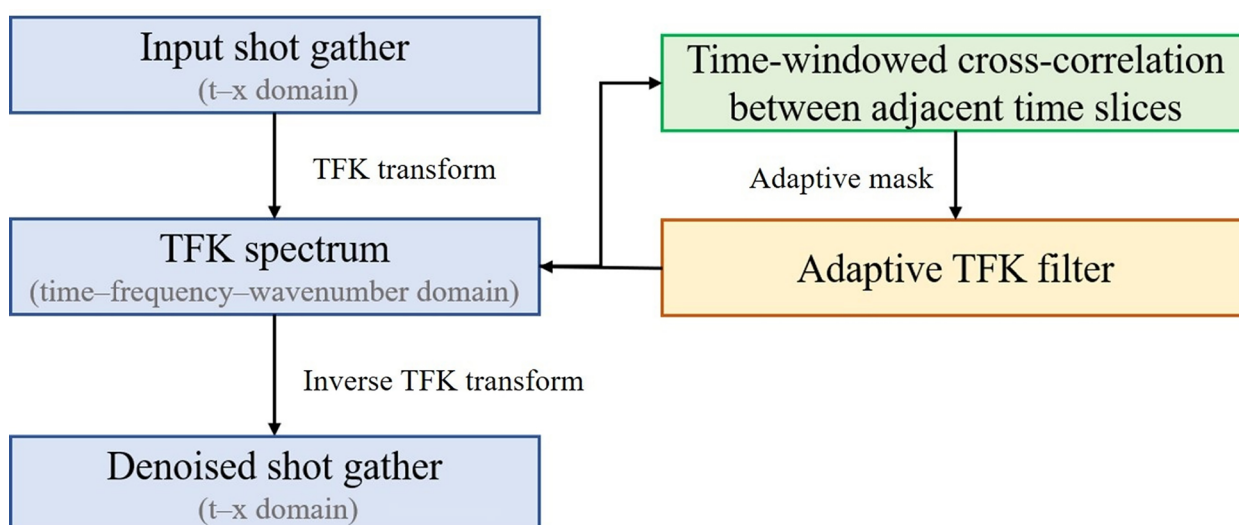


Figure 1. Flowchart of the proposed time-frequency-wavenumber (TFK) adaptive filter for surface-wave suppression

approach. The primary objective of this comparative analysis was to evaluate the relative performance of the two methods in suppressing dispersive surface wave energy while preserving useful reflection events. By applying both algorithms to the same dataset and examining their results in both the time and FK domains, the study aims to assess their differences in identifying surface wave components, maintaining the fidelity of practical reflections, and improving the overall signal-to-noise ratio. The insights gained from this comparison are intended to provide valuable guidance for the further optimization of surface-wave suppression strategies in seismic data processing.

3.1. Comparison of simulation data

In the synthetic experiment, a single-shot seismic record was constructed by superimposing a dispersive surface wave onto three hyperbolic reflection events. The reflected signals were assigned a dominant frequency of 20 Hz, while the surface wave was designed with a lower dominant frequency of approximately 10 Hz, mimicking a typical near-surface seismic scenario where low-frequency surface energy interferes with higher-frequency reflections. The sampling frequency was set to 200 Hz, and the total record length was 3.5 s, comprising 50 traces. The synthetic dataset was subsequently transformed into the FK domain using the FK transform (Figure 2).

As illustrated in Figure 2A, the time-domain single-shot record showed a nearly linear surface wave event that overlapped with the reflection signals, resulting in noticeable dispersion. The corresponding FK spectrum, shown in Figure 2B, revealed that the surface wave energy was distributed along a straight trajectory in the FK plane

and partially overlapped with the effective reflection energy band, exhibiting the typical low-frequency, high-amplitude characteristics of ground roll. This clear visualization allows for a direct assessment of the interaction between the surface and reflected waves in the spectral domain. Meanwhile, due to spatial sampling limitations in the dataset, pronounced spatial aliasing occurred, further exacerbating the overlap between the surface wave and effective wave energy in the FK spectrum. Consequently, the direct application of conventional FK filtering is prone to inadequate wave separation, leading to potential processing inaccuracies.

Building on this, a TFK transform was applied to the data to obtain a TFK spectrum, enabling a more detailed investigation of how surface wave energy evolves. FK spectra corresponding to different time instants were extracted to capture the temporal variability of the surface wave distribution. Because the FK spectrum is symmetric about the frequency axis, only the positive-frequency portion is presented here for clarity and conciseness.

Figure 3 illustrates the FK spectra obtained at three representative time instants: 0.5 s, 2 s, and 3 s. As shown, the spectra at 0.5 s and 3 s were dominated almost entirely by surface wave energy, while the spectrum at 2 s revealed a coexistence of both surface and reflection waves. This observation highlights the temporal overlap and complex interaction between dispersive ground roll and effective reflections, which pose a significant challenge for accurate separation and suppression in seismic data processing.

In this research, the energy of the signal waves was intentionally amplified relative to that of the surface waves, primarily to verify the stability of the proposed method

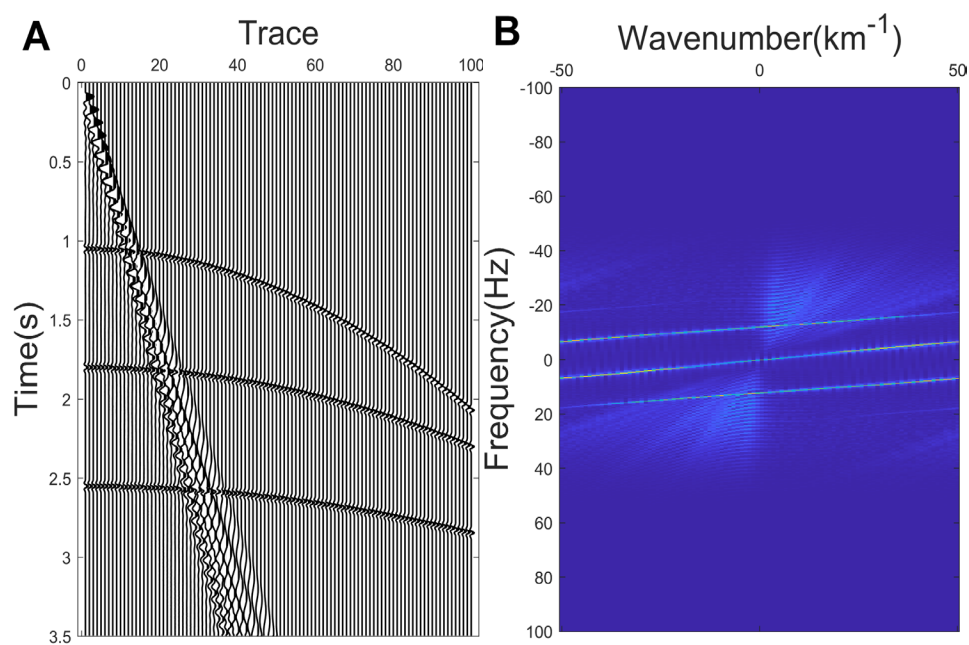


Figure 2. Generated data and corresponding frequency–wavenumber (FK) spectrum: (A) single-shot data and (B) FK spectrum of the synthetic data

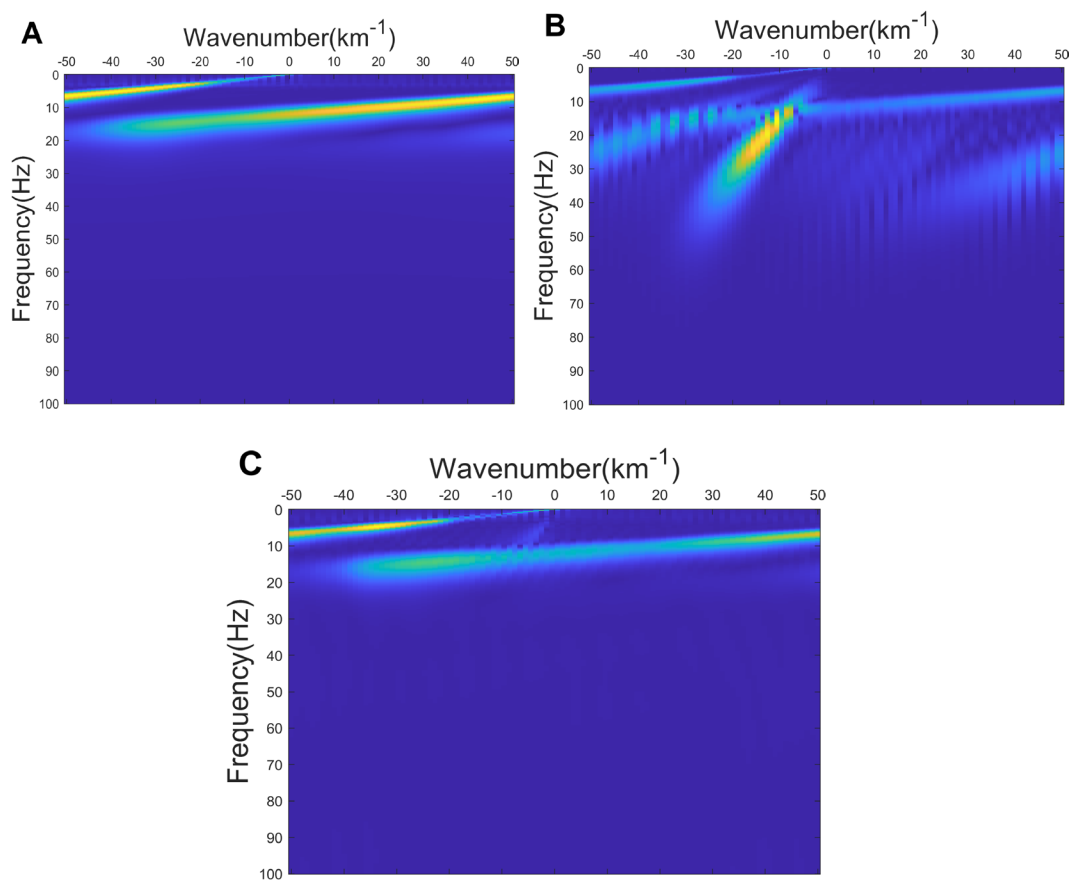


Figure 3. Frequency–wavenumber (FK) spectra at different time instants in the time–frequency–wavenumber transform. The FK spectral data at (A) 0.5 s, (B) 2 s, and (C) 3 s.

and to demonstrate that it relies not on energy magnitude but on energy distribution characteristics. As illustrated in Figure 3B, the energy of the signal waves was significantly higher than that of the surface waves, to the extent that it distorted the surface waves to a certain degree—this objectively increased the difficulty of extracting the surface wave region. Because surface waves are inherently dispersive, their FK spectra vary with time as the phase velocity changes with frequency. Although the distribution of surface wave energy exhibited slight differences across distinct time instants, the variations remained relatively minor within neighboring time windows. This property enables the implementation of a cross-correlation-based detection algorithm to identify regions dominated by surface wave energy, thereby enabling localized and adaptive suppression within the FK domain. In this research, we constructed a fan filter based on the surface wave velocity for FK filtering and then compared the results with those obtained via adaptive TFK filtering (Figure 4).

Figure 4 compares the performance of the conventional FK filter and the proposed adaptive TFK filter for both noise-free (Figure 4A–C) and noisy synthetic data (Figure 4D–F). In noise-free cases, the FK filter partially reduced surface wave energy while preserving the general trend of the reflection events. However, in regions where surface waves and reflections overlapped, the FK filter failed to achieve precise separation, leading to blurred reflection boundaries and residual low-frequency energy. This limitation is mainly due to the fixed-window nature of the FK domain, which limits its joint TF and spatial resolution and makes it difficult to completely suppress dispersive tail waves.

In noisy synthetic data cases, FK filtering showed strong residual surface wave energy and heavily contaminated reflections. In contrast, the adaptive TFK filter largely suppressed the coherent surface waves, and the remaining energy was mainly weak, incoherent background noise. The adaptive TFK filtering method introduced a joint TF analysis mechanism that dynamically adjusted the filtering response according to the local spectral characteristics of the data. This adaptive framework enables the algorithm to achieve a superior balance between waveform preservation and noise suppression, effectively reducing surface wave energy while maintaining the integrity of the reflection signals. Such improvements highlight the advantages of incorporating temporal adaptivity into surface-wave suppression procedures. Additionally, the residual random noise can be further suppressed by standard random-noise suppression techniques.

To further evaluate the surface-wave suppression performance of the two methods, FK spectra at different

time instants after filtering were analyzed and compared, as illustrated in Figure 5. Figure 5A–C shows the results obtained from the traditional FK filter, while Figure 5D–F displays the spectra derived from the adaptive TFK filtering approach. In the original dataset, the FK spectra at 0.5 s and 3 s were dominated by surface wave energy, whereas the spectrum at 2 s exhibited a mixture of surface and reflected waves.

As shown in Figure 5B, the conventional FK filtering method failed to eliminate the surface wave components. The suppression effect was primarily confined to the 0–10 Hz frequency range, beyond which substantial residual energy persisted. In regions where surface and reflection signals overlapped, the FK filter was largely ineffective, resulting in incomplete suppression.

By contrast, the adaptive TFK filtering method demonstrated superior performance: it effectively distinguished overlapping components and provided more thorough suppression of surface wave energy, even within mixed zones. Notably, in the FK spectrum at 2 s, the TFK approach retained the reflection signal to a greater extent while simultaneously suppressing the interfering surface waves. This outcome highlights that the proposed method exhibits excellent stability in surface wave region extraction and superior performance in surface wave suppression.

Figure 6 compares a single seismic trace (the 50th channel) before and after the application of the two filtering methods. As depicted, the FK method partially suppressed surface wave energy, but a substantial residual persisted at low frequencies. In contrast, the TFK approach demonstrated stronger suppression, with the surface wave component nearly eliminated from the record.

Nevertheless, a slight reduction in the amplitude of the reflection events was observed after TFK processing, indicating some degree of signal suppression. This issue can be mitigated by applying relative normalization or amplitude-compensation techniques during post-processing. Overall, the adaptive TFK filtering method achieved a more balanced trade-off between surface wave suppression and signal preservation, resulting in seismic records with improved clarity and enhanced signal-to-noise ratio. These findings confirm that incorporating TF adaptivity into the FK framework provides a more robust and flexible solution for addressing surface wave interference in seismic data processing.

In summary, the experimental results clearly demonstrate that the proposed adaptive TFK filtering method outperforms the traditional FK filtering technique in surface wave suppression. It effectively distinguishes and suppresses surface wave energy even within regions

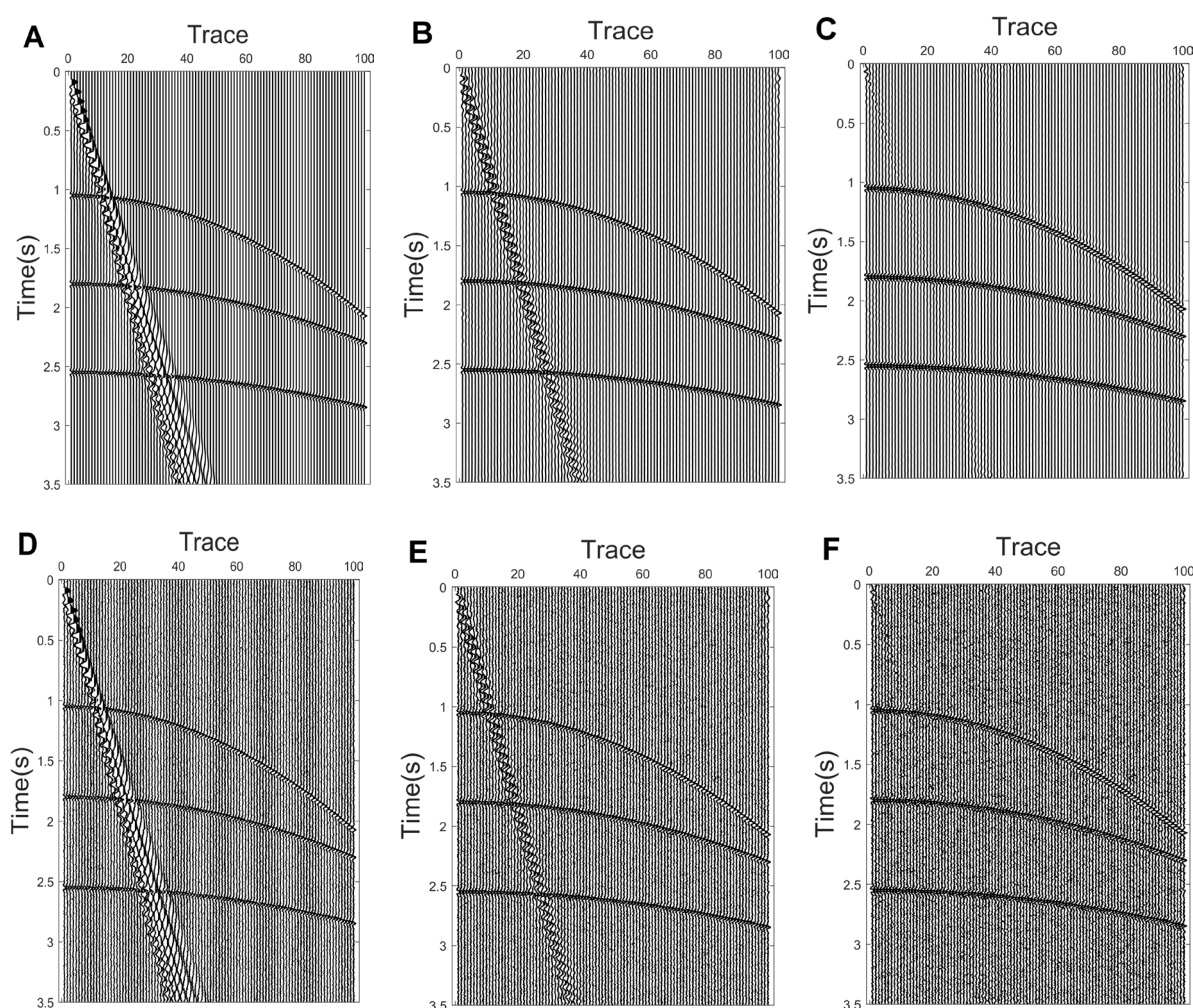


Figure 4. Comparison of frequency-wavenumber (FK) surface wave suppression and time-frequency-wavenumber (TFK) adaptive surface wave suppression: (A) Original noise-free synthetic data; (B) FK filtering results of (A); (C) adaptive TFK filtering results of (B); (D) original data with random noise; (E) FK filtering results of (D); and (F) adaptive TFK filtering results of (D)

affected by spatial aliasing and spatial overlap, while maintaining the integrity of the reflection signals. Beyond its improved suppression capability, the TFK approach enhances both the signal-to-noise ratio and the temporal-spatial resolution of the seismic data. These advantages underline its potential as a practical and powerful tool for seismic data processing under complex near-surface conditions, offering new perspectives for the development of adaptive, high-resolution filtering algorithms in applied geophysics.

3.2. Comparison of field data

To further evaluate the advantages of the proposed approach, two representative field seismic datasets were selected to compare the performance of the conventional FK filtering technique with the proposed adaptive TFK

filtering method in suppressing surface waves. Both datasets have a record length of 2 s and a sampling frequency of 500 Hz. [Figure 7](#) summarizes the raw seismic records from the two datasets, along with their corresponding one-sided FK spectra, which served as the basis for the subsequent comparison of filtering performance.

As illustrated in [Figure 7](#), surface wave energy dominated both field seismic datasets, with its intensity being significantly higher than that of effective reflection wave energy. Notably, the spatio-temporal distributions of surface waves differed between the two datasets: in Dataset 1 ([Figure 7A](#)), strong surface wave energy persisted throughout the entire time window, whereas in Dataset 2 ([Figure 7C](#)), it was concentrated locally and gradually attenuated over time. Further analysis of the unilateral FK spectrum revealed a distinct overlap

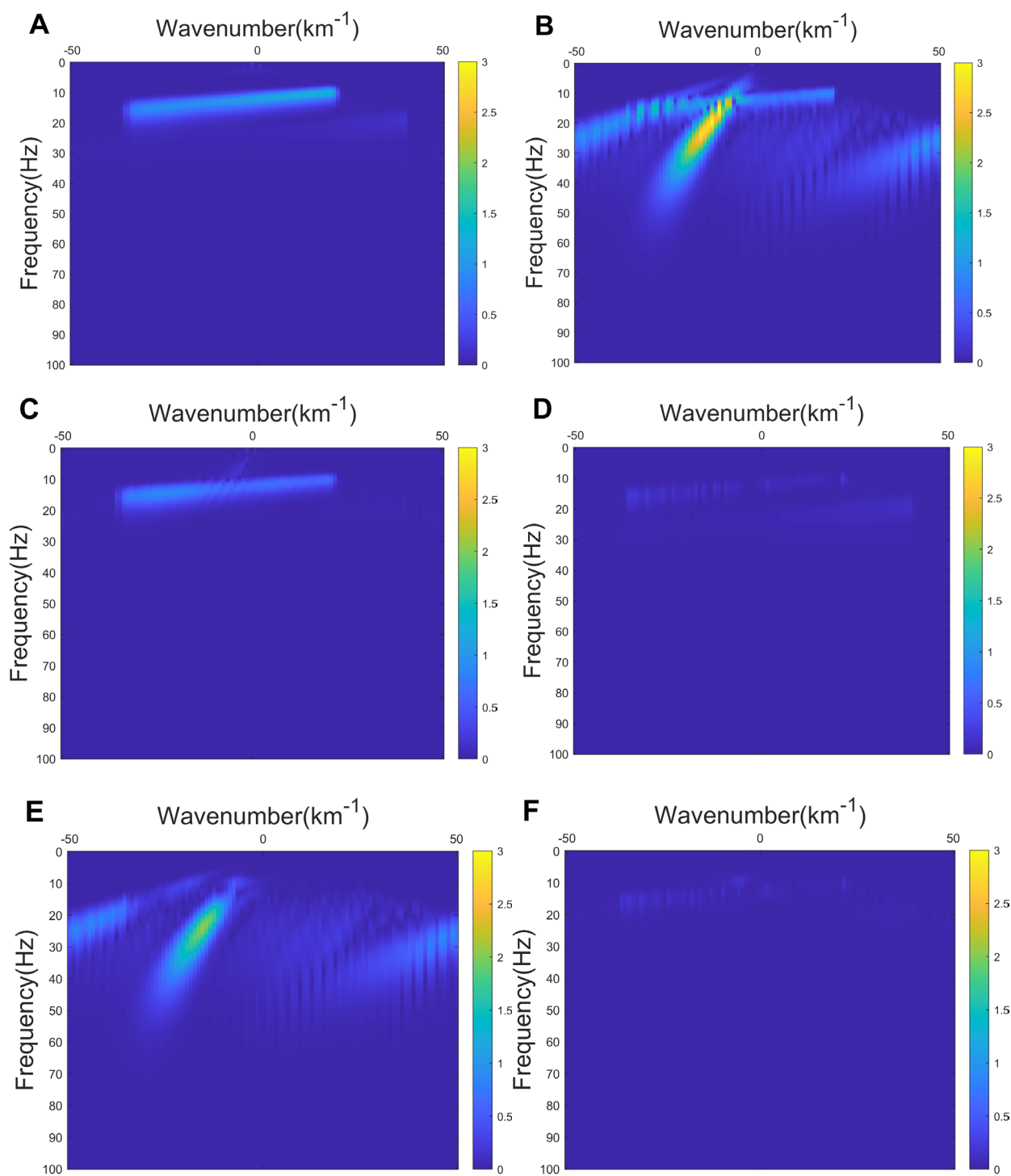


Figure 5. Distinct frequency–wavenumber (FK) spectra after suppression using two methods: (A–C) the FK spectrum at (A) 0.5 s, (B) 2 s, and (C) 3 s after FK filtering; and (D–F) the FK spectrum at (D) 0.5 s, (E) 2 s, and (F) 3 s after adaptive time–frequency–wavenumber filtering

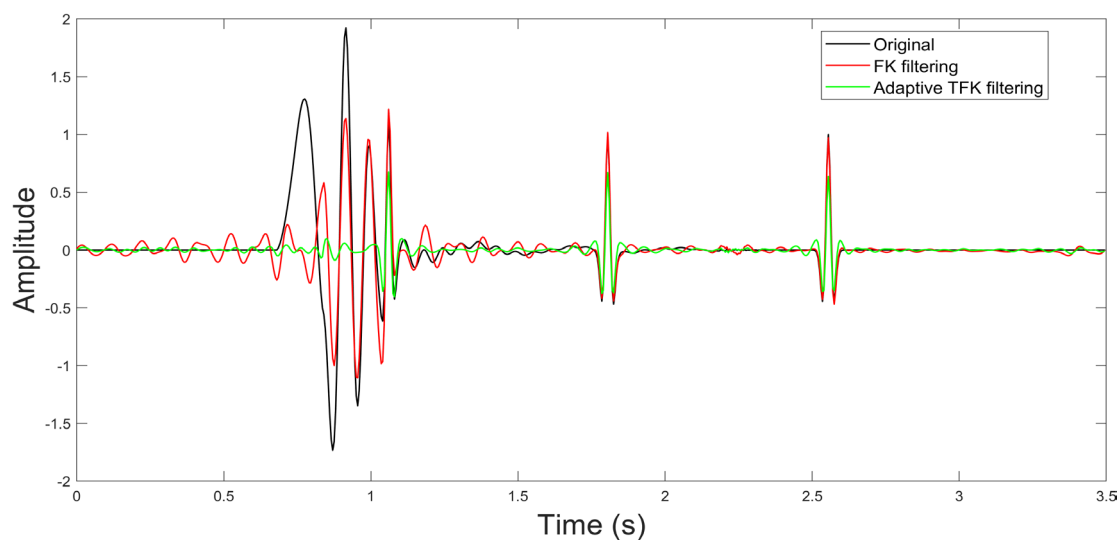


Figure 6. Comparison of frequency-wavenumber (FK) spectra after suppression: original data (black line), FK filtering (red line), and adaptive time-frequency-wavenumber (TFK) filtering (green line)

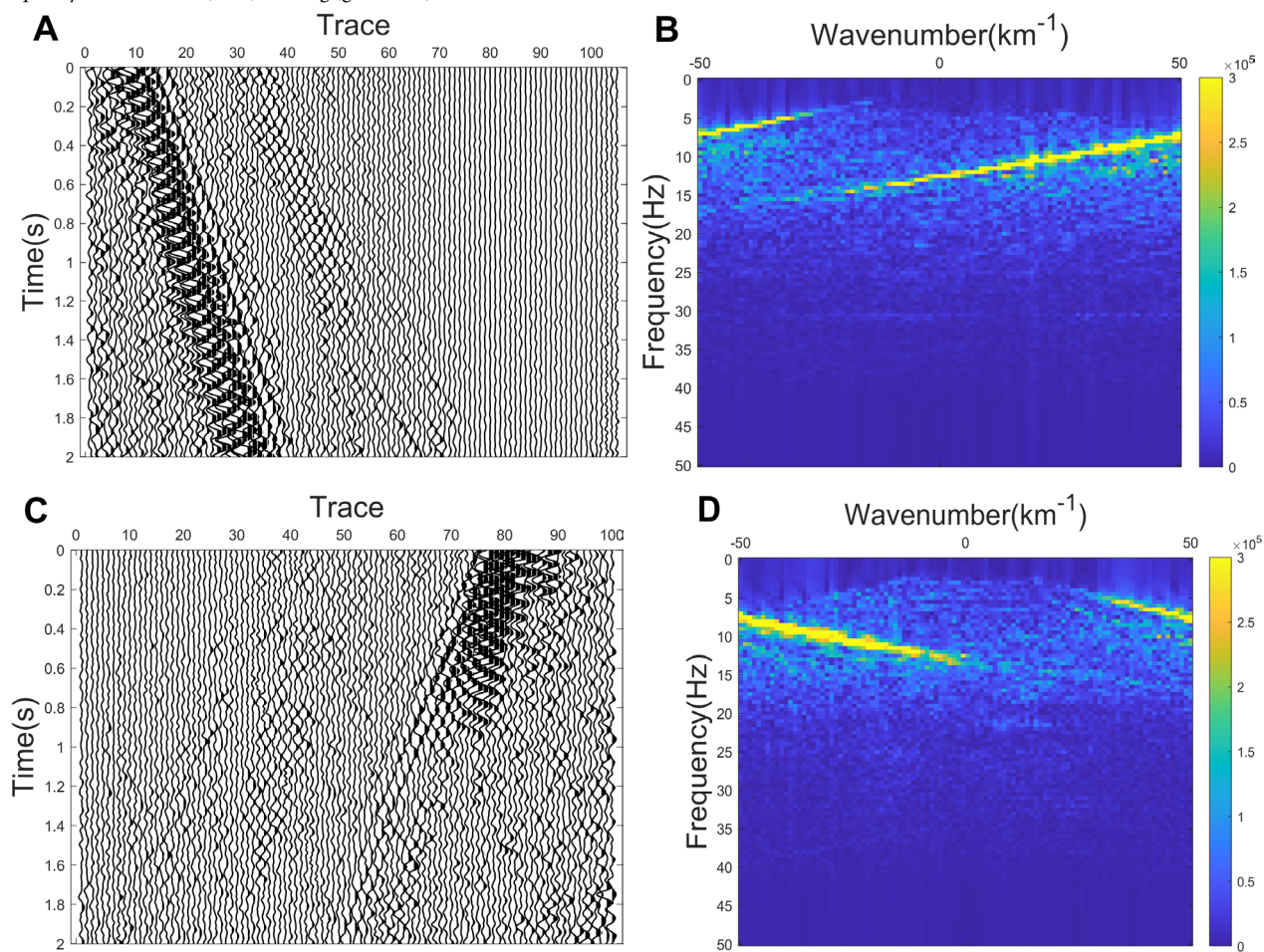


Figure 7. Two field seismic datasets and their corresponding one-sided frequency-wavenumber (FK) spectra. (A) Field seismic data (Dataset 1). (B) One-sided FK spectrum of Dataset 1. (C) Field seismic data (Dataset 2). (D) One-sided FK spectrum of Dataset 2.

between the dominant frequency bands of surface waves and reflection waves. Under such circumstances, it is challenging to delineate a clear separation cone in the FK domain, which renders traditional FK filtering ineffective for surface wave suppression. To address this issue, this study employed the proposed adaptive TFK filtering to process the two datasets. Figure 8 presents the filtering results of the two methods and their corresponding FK spectra, enabling an intuitive comparison of their surface-wave suppression performance and the associated spectral energy distribution characteristics.

For Dataset 1, Figure 8A shows the processing results of traditional FK filtering, while Figure 8B presents those of adaptive TFK filtering. For Dataset 2, Figure 8C,D displays the filtering results under the condition of mirror extension, where Figure 8C corresponds to traditional FK filtering and Figure 8D to adaptive TFK filtering. Boundary artifacts can be effectively mitigated by performing mirror extension and then extracting the region corresponding to

the original dataset. By comparing Figure 8A with Figure 8B, and Figure 8C with Figure 8D, it can be observed that, compared with traditional FK filtering, adaptive TFK filtering achieved more significant surface wave suppression in both datasets. Meanwhile, it better preserved the continuity and integrity of reflection wave events, thus reducing damage to effective signals. A comparison between Figure 8B and Figure 8D demonstrated that adaptive TFK filtering exhibited superior surface-wave suppression performance to traditional FK filtering when mirror extension was applied. In contrast, traditional FK filtering suffered from obvious residual surface waves and energy dispersion, whereas the TFK method more effectively concentrated and suppressed surface wave energy.

The unilateral FK spectra in Figure 9 indicate significant energy overlap between surface and reflection waves in the FK domain for both field datasets, making it difficult for traditional FK filtering to achieve effective separation

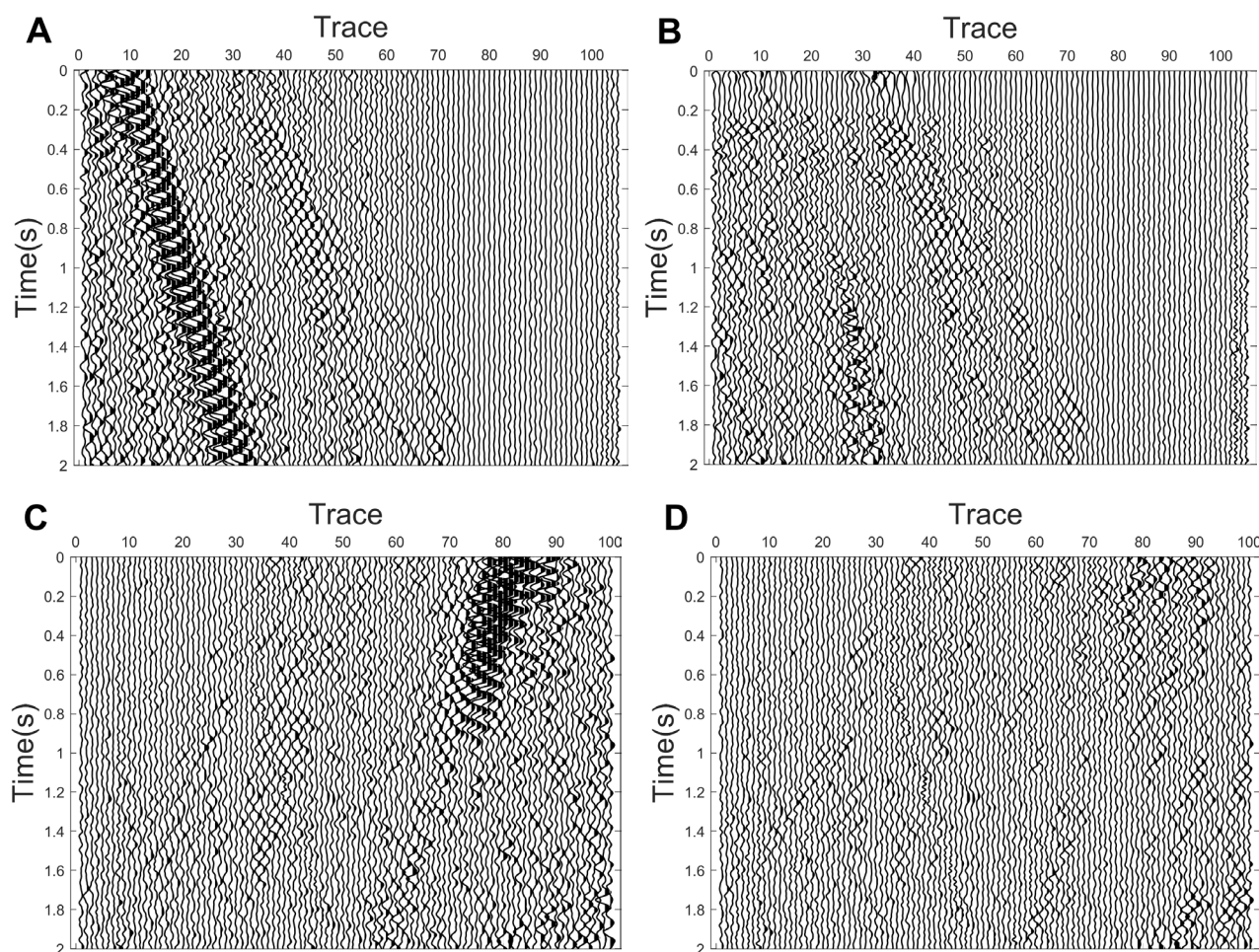


Figure 8. Surface-wave suppression results from the two field seismic datasets. (A) Frequency–wavenumber (FK) filtering on Dataset 1. (B) Adaptive time–frequency–wavenumber (TFK) filtering on Dataset 1. (C) FK filtering on Dataset 2. (D) Adaptive TFK filtering on Dataset 2.

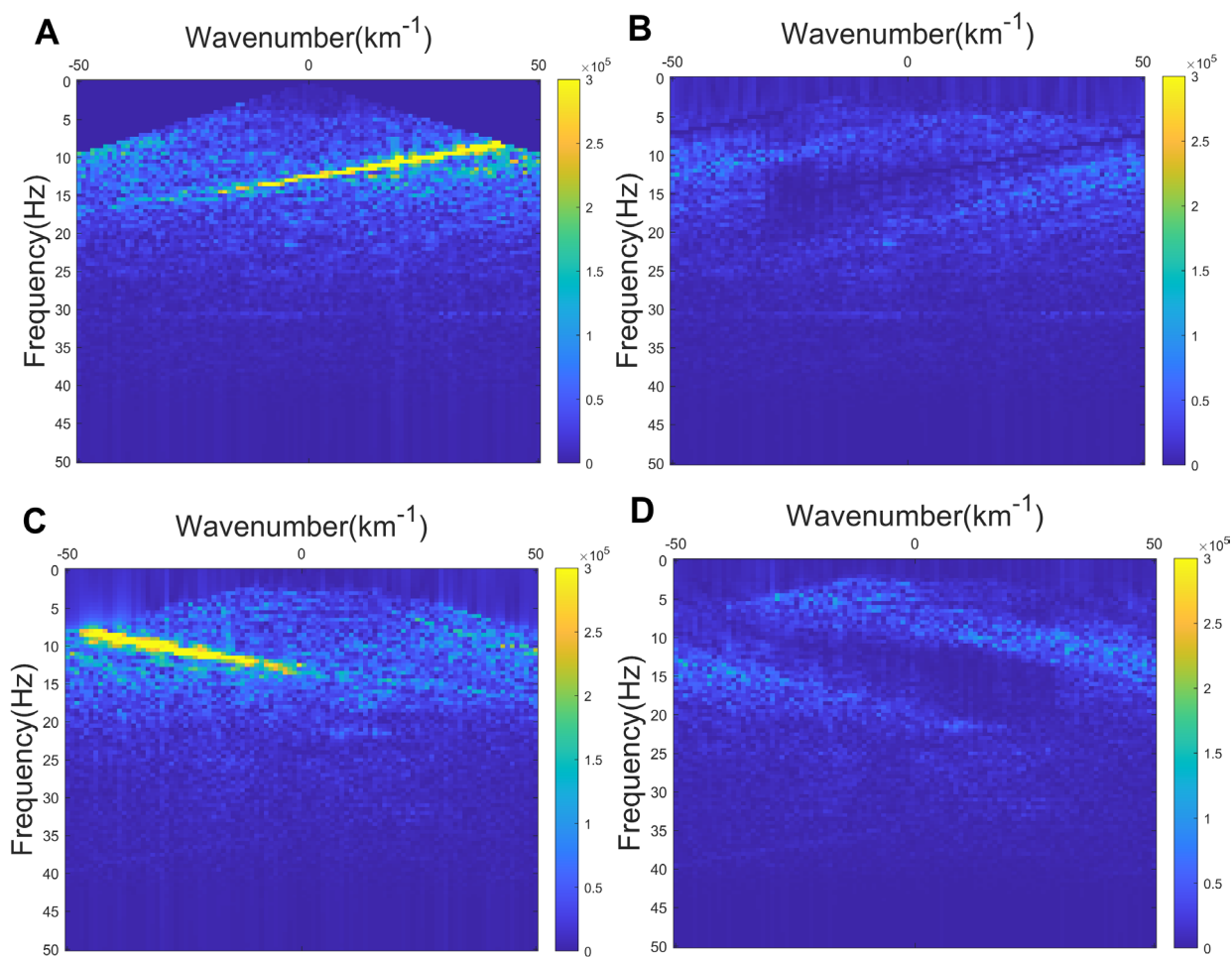


Figure 9. Comparison of FK filtering and adaptive time-frequency-wavenumber (TFK) filtering for the two field seismic datasets. (A) FK filtering on Dataset 1. (B) Adaptive TFK filtering on Dataset 1. (C) FK filtering on Dataset 2. (D) Adaptive TFK filtering on Dataset 2.

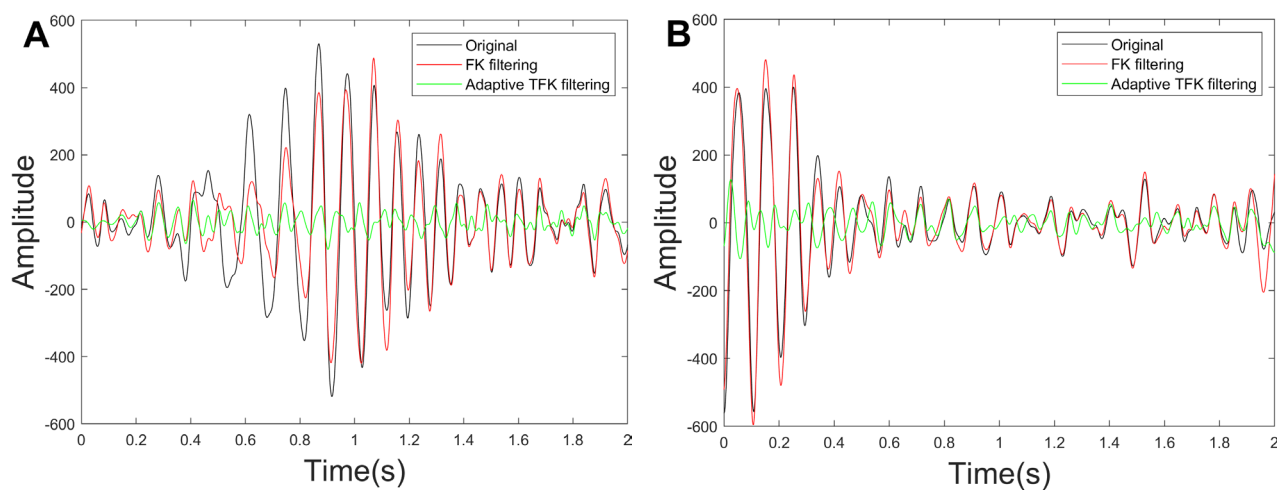


Figure 10. Comparison of frequency-wavenumber (FK) spectra after suppression in (A) the 20th trace from Dataset 1 and (B) the 80th trace from Dataset 2: original data (black line), FK filtering (red line), and adaptive time-frequency-wavenumber (TFK) filtering (green line)

without compromising reflection signals. By introducing the temporal dimension, adaptive TFK filtering improved the ability to characterize non-stationary energy distributions, thereby alleviating the aforementioned overlap issue to a certain extent and enabling more efficient surface wave suppression.

To provide a more precise trace-level comparison of filtering performance, representative traces were extracted from the two field datasets for detailed analysis (Figure 10): the 20th trace from Dataset 1 and the 80th trace from Dataset 2. For the 20th trace of Dataset 1 (Figure 10A), surface wave energy was mainly concentrated within 0.4–1.4 s, where the original record exhibited large amplitudes. Conventional FK filtering suppressed the surface waves only partially, leaving noticeable residuals. In contrast, the adaptive TFK filter yielded stronger suppression in this interval. Outside the surface wave window (0–0.4 s and 1.4–2 s), which was dominated by reflections, waveform

changes were minor, indicating that the proposed method suppresses surface waves while preserving reflection events.

For the 80th trace of Dataset 2 (Figure 10B), surface wave energy was primarily distributed within 0–0.6 s. Conventional FK filtering again left residual surface wave energy, whereas the adaptive TFK filter provided further suppression. In the 0.6–2 s interval, the waveforms were largely preserved, suggesting limited distortion to effective signals. Overall, consistent improvements on representative traces from both datasets support the robustness and generality of the proposed approach.

To further evaluate the effectiveness of surface wave suppression, stacked sections from the unprocessed data, the conventional FK-filtered results, and the proposed adaptive TFK-filtered results were generated and compared (Figure 11). In the unprocessed data, strong surface waves appeared as high-amplitude, highly coherent noise bands,

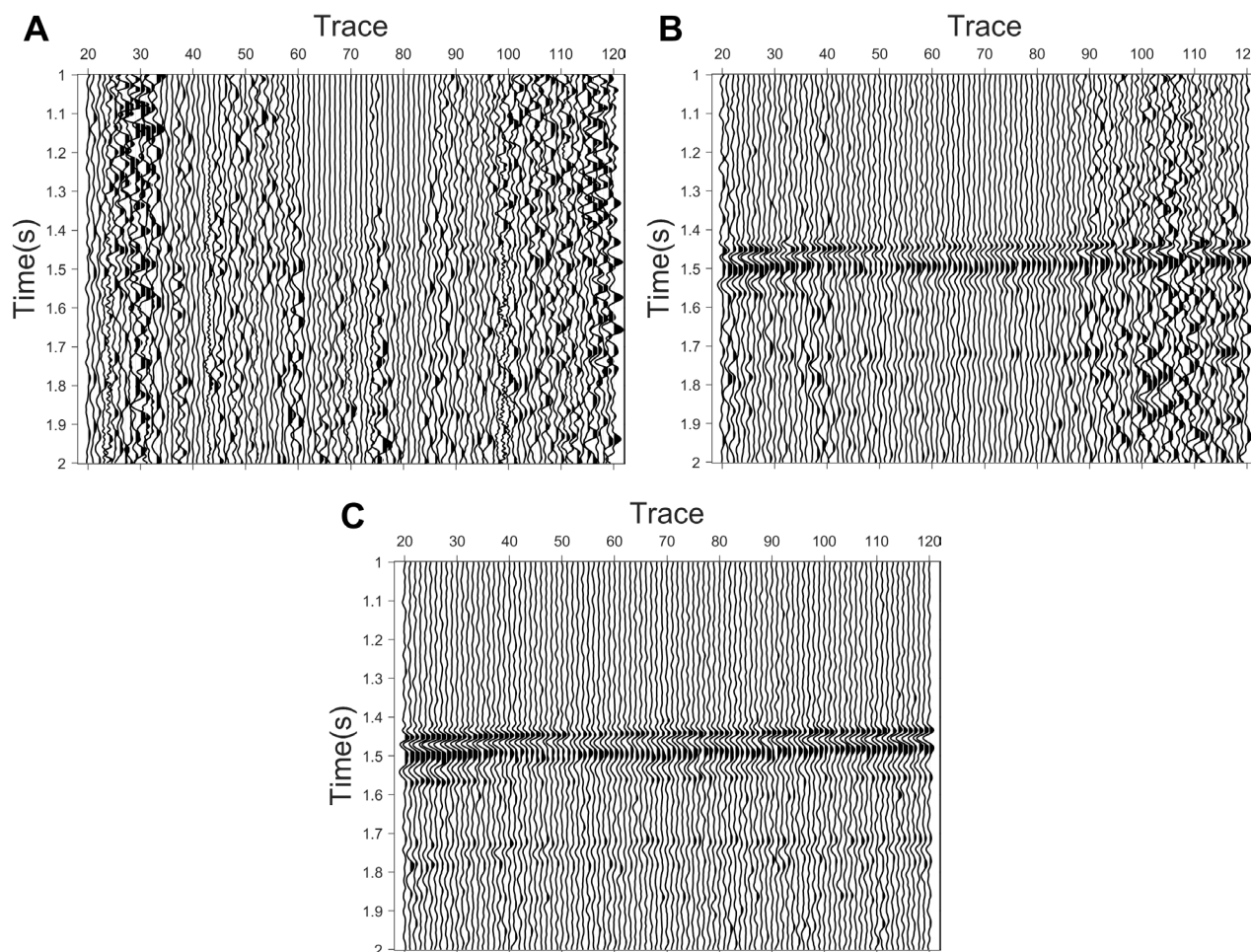


Figure 11. Profile comparison of surface wave suppression using different methods: (A) unprocessed data; (B) data after conventional frequency-wavenumber filtering; (C) data after the adaptive time-frequency-wavenumber filtering

severely obscuring reflection events and hindering reliable identification and tracking of reflection coherency. After applying the conventional FK filter, the primary reflection events became discernible; however, noticeable residual surface wave energy persisted, accompanied by locally degraded phase continuity. In contrast, the data obtained with the adaptive TFK filter showed further suppression of residual surface wave bands, with markedly improved continuity and traceability of reflection events. These observations indicate that the proposed method can more effectively suppress surface wave interference while largely preserving the dominant morphology and phase characteristics of the useful reflected signals.

In summary, the comparative results in [Figures 8–11](#) demonstrate that, for field data in which surface wave and reflection energies overlap substantially in the FK domain, conventional FK filtering often fails to simultaneously achieve effective surface wave suppression and preserve reflection continuity. By incorporating the time dimension, the proposed adaptive TFK filtering leverages correlations between FK spectra from adjacent time windows to provide a data-driven characterization of surface wave-dominated regions. This enables a more effective spectral suppression of surface wave energy and its aliasing/mixing with reflection bands, while yielding reduced residual surface wave artifacts and more continuous, traceable reflection events at both the gather and stacked-section scales. These results validate the feasibility of targeted suppression in the TFK domain by exploiting differences in the time-varying spectral distributions of surface waves and reflections, and further suggest a more robust implementation pathway for adaptive surface wave suppression under complex field-acquisition conditions.

This study also conducted an efficiency comparison between the proposed method and FK filtering, focusing on processing efficiency under both simulated and field datasets. In principle, the TFK method operates via an FK transformation in the TFK domain, resulting in lower efficiency than conventional FK filtering. However, due to its parallelizable computational process, the method still holds substantial potential to improve efficiency in practical data processing. The computational time statistics are presented in [Table 1](#).

Table 1. Efficiency comparison

Sample	FK filter (s)	TFK filter (s)
Dataset 1	0.01	3.90
Dataset 2	0.20	4.50

Abbreviations: FK: Frequency–wavenumber; TFK: Time–frequency–wavenumber.

As shown in [Table 1](#), the TFK filtering method performed worse in single-core processing. However, in practical processing scenarios, it can still leverage GPU parallel computing, thereby alleviating this inefficiency to a certain extent.

4. Discussion

In this research, an adaptive TFK filtering method for surface wave suppression was proposed. The core idea of this approach is to construct an adaptive filter by cross-correlating spectral components in the FK domain across successive time intervals. This filter dynamically adjusts its characteristics in response to temporal variations in the seismic data, thereby better capturing the non-stationary nature of surface waves. After processing data in the FK domain, an inverse transform is applied to reconstruct the time-domain seismic records, preserving relative signal characteristics while effectively reducing surface wave energy. The key findings are as follows:

- (i) Effectiveness in simulated data: The analysis of simulated datasets demonstrates that the proposed method can efficiently and automatically identify the spatial and spectral locations of surface waves within the FK domain. By adaptively adjusting filter parameters across different time windows, the method achieves enhanced discrimination between surface and effective waves. Compared with the conventional FK filtering technique, the proposed approach considerably simplifies the workflow by eliminating the need for repeated manual parameter tuning. Furthermore, it achieves rapid and accurate localization of surface waves, leading to more complete suppression of dispersive surface energy while maintaining the fidelity of the effective signal. Here, the term *fidelity* refers to the preservation of relative amplitude relationships of effective signals, rather than strict absolute amplitude preservation.
- (ii) Improved stability and adaptability: Because the filter adapts dynamically with time, the method exhibits significantly improved stability and robustness. It can effectively accommodate temporal variations and changes in the statistical characteristics of seismic data, thereby ensuring more consistent performance across different datasets and acquisition conditions. This adaptability also reflects the intrinsic time-varying behavior of surface waves, implying that multi-scale and time-dependent information must be incorporated for efficient suppression. Consequently, the adaptive TFK method not only enhances the stability of the filtered data but also broadens the technique's applicability to a broader

range of geological settings and survey environments.

- (iii) Superior performance in field data: When applied to real seismic field data, comparative analysis with traditional FK filtering further confirms the advantages of the proposed adaptive TFK approach. It demonstrates greater robustness in handling complex field conditions, effectively reducing surface wave interference while retaining weak yet interpretable effective signal components. The method requires fewer empirical adjustments and operates with acceptable computational efficiency for practical applications, while producing cleaner seismic records with improved signal-to-noise ratios. Overall, the adaptive TFK surface-wave suppression technique provides a practical, theoretically sound solution with acceptable processing efficiency for mitigating surface wave contamination in both simulated and field seismic datasets.
- (iv) Limitations and future research directions: Notably, higher-mode surface waves were not removed in the present study. The core focus of this research is the suppression of high-energy surface waves, which are the primary source of interference affecting the quality of target reflected signals in seismic data processing. Within the datasets employed in this work (both simulated and field data), higher-mode surface waves exhibit relatively weak energy, exerting minimal impact on overall data interpretation. Therefore, effective extraction and suppression of higher-mode surface waves—particularly in scenarios where such modes are prominent—would require further investigation. Future efforts could focus on refining the adaptive identification logic in the TFK domain, tailoring key parameters to the energy and propagation features of low-energy higher-mode waves, or incorporating specialized modal separation mechanisms into the existing framework.

5. Conclusion

This study presents an adaptive TFK approach for surface wave suppression in seismic data. This method introduces a dynamic filtering framework that accounts for the time-varying and dispersive characteristics of surface waves, thereby achieving more accurate and adaptive noise suppression.

The findings indicate that the adaptive TFK method not only enhances surface wave suppression but also preserves the relative amplitude characteristics of effective signals. By constructing a time-dependent filtering strategy in the FK domain and integrating TF optimization, the approach demonstrates strong adaptability and stability

across various seismic conditions. These improvements contribute to more reliable data for subsequent imaging and inversion tasks.

The proposed technique provides a practical and efficient alternative to conventional FK filtering, reducing the need for manual parameter adjustments and offering greater robustness in complex field-acquisition environments. Its flexibility and computational efficiency make it a promising tool for modern seismic data processing workflows.

Acknowledgments

None.

Funding

This research was supported by the Open Fund of the SINOPEC Key Laboratory of Geophysics (Grant No. 36750000-24-FW0399-0004), the Natural Science Foundation of Xinjiang Uygur Autonomous Region (Grant No. 2022D01C659) under the “Tianchi Talent” Introduction Program, and the Open Fund of Northwest Oilfield Branch Company, SINOPEC (Grant No. 34400000-25-ZC0607-0156).

Conflict of interest

The authors declare they have no competing interests.

Author contributions

Conceptualization: Yong Wang

Formal analysis: Yong Wang, Xuejie Gao

Investigation: Xuejie Gao, Zerun Nian, Lang Yang

Methodology: Yong Wang, Youjuan He, Zhili Chen

Writing—original draft: Xuejie Gao

Writing—review & editing: Youjuan He

Availability of data

Data associated with this research are available and can be obtained by contacting the corresponding author.

References

1. Zheng JJ, Yin XY, Zhang GZ, Wu GH, Zhang ZS. The surface wave suppression using the second generation curvelet transform. *Appl Geophys*. 2010;7(4):325–335.
doi: 10.1007/s11770-010-0257-x
2. Wang D, Li Z, Huang J, Dong L, Ding C. Surface wave suppression based on the characteristic of reflected wave. In: *Proceedings of Beijing 2014 International Geophysical Conference & Exposition*; 21–24 April 2014; Beijing, China. Society of Exploration Geophysicists and Chinese Petroleum Society; 2014:307–310.
doi: 10.1190/igcbeijing2014-079

3. Lv S, Gong X, Hu B, Xu Z, Zhang J, Cheng Q. Adaptive non-subsampled shearlet transform and its application to surface wave suppression. *IEEE Trans Geosci Remote Sens.* 2024;62:1–15.
doi: 10.1109/TGRS.2024.3477954
4. Li Q, Shen A, Guo Y, Wu J, Shi Y. Review of evaluating asphalt pavement structure integrity and strength with Rayleigh wave methods: techniques, applications, and trends. *Measurement.* 2024;234:114849.
doi: 10.1016/j.measurement.2024.114849
5. Tokeshi J, Karkee CK, Sugimura Y. Reliability of Rayleigh wave dispersion curve obtained from f–k spectral analysis of microtremor array measurement. *Soil Dyn Earthq Eng.* 2006;26(2–4):163–174.
doi: 10.1016/j.soildyn.2005.02.013
6. Kong XL, Chen H, Hu ZQ, Kang JX, Xu TJ, Li LM. Surface wave attenuation based on polarization attributes in time-frequency domain for multicomponent seismic data. *Appl Geophys.* 2018;15(1):99–110.
doi: 10.1007/s11770-018-0656-y
7. Rasol MA, Pérez-Gracia V, Fernandes FM, Pais JC, Santos-Assunção S, Santos C, Sossa VG. GPR laboratory tests and numerical models to characterize cracks in cement concrete specimens exemplifying damage in rigid pavement. *Measurement.* 2020;158:107662.
doi: 10.1016/j.measurement.2020.107662
8. Meng A, Xu H, Feng X, Tan Y. Feasibility of freeze-thaw damage analysis for asphalt mixtures through dynamic nondestructive testing. *Constr Build Mater.* 2020;233:117220.
doi: 10.1016/j.conbuildmat.2019.117220
9. Wang X, Huang H, Shen S, Jin G, Mao Q, Lu H. Characterization of in situ modulus of asphalt pavement and its relation to cracking performance using SASW method. *J Transp Eng Part B Pavements.* 2020;146(3):04020039.
doi: 10.1061/JPEODX.0000195
10. Yuanyuan H, Rui Y, Jishun P, Xin L. A 3D surface wave attenuation method based on dispersion curve analysis and its application. *Acta Geophys.* 2024;72(6):4123–4138.
doi: 10.1007/s11600-024-01318-2
11. Serdyukov AS, Yablokov AV, Duchkov AA, Azarov AA, Baranov VD. Slant f–k transform of multichannel seismic surface wave data. *Geophysics.* 2019;84(1):A19–A24.
doi: 10.1190/geo2018-0430.1
12. Serdyukov AS. Ground-roll extraction using the Karhunen–Loeve transform in the time-frequency domain. *Geophysics.* 2022;87(2):A19–A24.
doi: 10.1190/geo2021-0453.1
13. Zheng Y, He DK, Feng X. Surface wave suppressing and decomposition using deep neural networks. In: Proceedings of 83rd EAGE Annual Conference & Exhibition; 6–9 Jun 2022; Madrid, Spain. European Association of Geoscientists & Engineers; 2022:1–5.
doi: 10.3997/2214-4609.202210218
14. Jin Z, Li G, Ou G. Improvement of inverse dispersion technique for ground roll attenuation in sedimentary environment. *J Appl Geophys.* 2024;220:105268.
doi: 10.1016/j.jappgeo.2023.105268
15. Liu S, Birnie C, Bakulin A, Dawood A, Silvestrov I, Alkhalifah T. A self-supervised scheme for ground roll suppression. *Geophys Prospect.* 2024;72(7):2580–2598.
doi: 10.1111/1365-2478.13522
16. Son YH, Park H, Cho Y, Min DJ. Ground-roll attenuation using dual-model self-supervised selective learning with blind horizontal convolutional neural networks. *J Appl Geophys.* 2024;224:105363.
doi: 10.1016/j.jappgeo.2024.105363
17. Yablokov AV, Moiseev MV, Serdyukov AS, Litvichenko DA. Algorithm for surface wave suppression on 2D seismic data using the slant Karhunen–Loeve transform in a time-frequency domain. *Russ Geol Geophys.* 2024;65(5):650–662.
doi: 10.2113/RGG20234660
18. He XL, Liu SQ, Tong ZQ. 3-D denoising method through visual speed in frequency–wavenumber domain. *J China Univ Pet (Nat Sci Ed).* 2010(4):62–66. [In Chinese].
doi: 10.3969/j.issn.1673-5005.2010.04.011
19. Tian Y, Wang X, Peng G, Wang X, Su Q. Noise attenuation technology on wide azimuth seismic data. *Oil Geophys Prospect.* 2013;48(2):187–191. [In Chinese].
doi: 10.13810/j.cnki.issn.1000-7210.2013.02.013
20. Askari R, Siahkoobi HR. Ground roll attenuation using the S and x–f–k transforms. *Geophys Prospect.* 2008;56(1):105–114.
doi: 10.1111/j.1365-2478.2007.00659.x
21. Liu Y, Fomel S. Seismic data analysis using local time–frequency decomposition. *Geophys Prospect.* 2013;61(3):516–525.
doi: 10.1111/j.1365-2478.2012.01062.x
22. Wang C, Wang Y. Ground roll attenuation using polarization analysis in the t–f–k domain. *Geophys J Int.* 2017;210(1):240–254.
doi: 10.1093/gji/ggx152
23. Wu Y, Pan S, Yi S, Chen J, Cui Q, Song G. An automatic screening method for the passive surface-wave imaging based on the F–K domain energy characteristics. *IEEE Trans Geosci Remote Sens.* 2023;61:1–12.
doi: 10.1109/TGRS.2023.3321786

-
24. Sun H, Liu E, Zhang F, Wang W, Li X. Seismic shear wave noise suppression and application to well tie. *J Geophys Eng.* 2024;21(6):1619–1635.
doi: 10.1093/jge/gxae091
 25. Stockwell RG, Mansinha L, Lowe RP. Localization of the complex spectrum: the S transform. *IEEE Trans Signal Process.* 1996;44(4):998–1001.
doi: 10.1109/78.492555
 26. Xu S, Zhang Y, Lambaré G. Antileakage Fourier transform for seismic data regularization in higher dimensions. *Geophysics.* 2010;75(6):WB113–WB120.
doi: 10.1190/1.3507248.